Available online at www.sciencedirect.com
ScienceDirect
ELSEVIER
April 2015, 22(2): 89–95
www.sciencedirect.com/science/journal/10058885
The Journal of China Universities of Posts and Telecommunications
http://jcupt.xsw.bupt.cn

Compressed sensing based multi-rate sub-Nyquist sampling system

Xiong Yanwei (✉), Zhang Jianhua, Zhang Ping

Key Laboratory of Universal Wireless Communication, Beijing University of Post and Telecommunications, Beijing 100876, China

Abstract

Signal sampling is a vital component in modern information technology. As the signal bandwidth becomes wider, the sampling rate of analog-to-digital conversion (ADC) based on Shannon-Nyquist theorem is more and more high and may be beyond its capacity. However the analog to information converter (AIC) based on compressed sensing (CS) is designed to sample the analog signals at a sub-Nyquist sampling rate. A new multi-rate sub-Nyquist sampling (MSS) system was proposed in this article, it has one mixer, one integrator and several parallel ADCs with different sampling rates. Simulation shows the signals can be reconstructed in high probability even though the sampling rate is much lower than the Nyquist sampling rate.

Keywords CS , sub-Nyquist rate, AIC, MSS

1 Introduction

With rapid development of wireless communication technology, the demand for information is increasing dramatically. The signal bandwidth becomes wider and wider to satisfy the increasing data volume. In traditional digital signal processing which inherently relies on sampling process, the ADC requires the sampling rate must be at least twice of the bandwidth according to the Shannon-Nyquist theorem to guarantee the reconstruction of the band-limited signal. The high frequency and high resolution ADC is one of the main performance limiters in advanced communication applications, where the bandwidth is high and the sampling rate is beyond the capacity of ADC. In the case of the research based on traditional ADC, the acquisition hardware, the subsequent storage and digital signal processors are facing with great challenges.

Periodic non-uniform sampling is a popular approach to reduce the sampling rate. Multicoset sampling is a specific strategy of this type [1]. Instead of implementing a single ADC at a high Nyquist sampling rate f_{NYQ}, interleaved ADCs use P devices at rate f_{NYQ}/P with appropriate time shifts. However, time interleaving has two fundamental limitations. First, the P low-rate samplers have to share an analog front-end which must tolerate the input bandwidth f_{NYQ}. With today's technology the possible front-ends are still far below the wideband regime. Second, maintaining accurate time shifts, on the order of $1/f_{\mathrm{NYQ}}$, is difficult to implement.

Fortunately, recent work in CS provided ways to sample sparse or compressible signals efficiently at a sub-Nyquist rate [2–3]. CS suggested that the signal characteristics could be fully captured by a number of projections which are fewer than those required by Nyquist theorem and reconstructed from them lossless. CS reveals a useful theorem that the sampling rate is determined based on the actual information contents rather than the signal bandwidth. This theorem has found a wide range of applications in communication, such as channel estimation, sensor network and cognitive radio.

Kinds of practical methods to implement the AIC for sampling at a sub-Nyquist rate were presented [4–8]. AIC usually consists of three main components: demodulation, integral and uniform sampling. [4] extended the exiting CS framework to analog signals and the AIC has only one path. Another practical sampling system which was inspired by Ref. [4] was presented in Ref. [5], it consists of a bank of

Received date: 21-03-2014
Corresponding author: Xiong Yanwei, E-mail: cherryxiong86@gmail.com
DOI: 10.1016/S1005-8885(15)60644-6

random demodulators and ADCs running in parallel. The corresponding shows that this system has much lower sampling rate but consumes much resource if the architecture contains a large number of parallel paths.

In order to provide design flexibility and scalability, a parallel segmented compressed sensing (PSCS) structure was adopted [6–8]. The original signals are segmented and simultaneously transmitted to several parallel paths, then are fed into output after demodulation, piecewise integral and low speed sampling. PSCS reduces the number of paths by increasing the sampling rate. But it still has several parallel paths which are independent of each other. Each path has separated demodulation, piecewise integral and uniform sampling. PSCS structure consume much resources if a large number of parallel paths are contained.

A new MSS system was proposed in this article to make the AIC be easily implemented. Its architecture only has one multiplier and one integrator. The original signals are first demodulated and integrated during the whole signal period, and then are simultaneously sent to different ADCs to be sampled at different rates. Compared with PSCS structure, this architecture is simpler and consumes fewer resources.

The remainder of this article is organized as follows. In Sect. 2 we introduce the multicoset sampling and AIC background. Sect. 3 describes the MSS system and gives some analysis. Simulation results are shown in Sect. 4 and conclusions are made in Sect. 5.

2 Multicoset sampling and AIC background

2.1 Multicoset sampling

Multicoset sampling involves periodic nonuniform sampling of the Nyquist-rate sequence $x(nT_{\mathrm{NYQ}})$, where $T_{\mathrm{NYQ}}=1/f_{\mathrm{NYQ}}$. Let P be a positive integer, and $C=\{c_p\}_{p=1}^{P}$ be a set of p distinct integers with $0\leqslant c_p\leqslant P-1$. Multicoset samples consist of p uniform sequences, called cosets, with the pth coset defined by

$$x_{c_p}[n]=x(nPT_{\mathrm{NYQ}}+c_pT_{\mathrm{NYQ}});\quad n\in\mathbb{Z} \tag{1}$$

Only $p<P$ cosets are used, so that the average sampling rate is $p/(PT_{\mathrm{NYQ}})$, lower than the Nyquist sampling rate.

A possible implementation of the multicoset sampling is depicted in Fig. 1. The building blocks are p uniform samplers at rate $1/(PT_{\mathrm{NYQ}})$, where the ith sampler is shifted by c_pT_{NYQ} from the origin. Although this scheme seems intuitive and straightforward, ADCs practically introduces an inherent bandwidth limitation, which distorts the samples. To avoid these distortions, an ADC with matching the Nyquist rate of the input signal must be used, even if the actual sampling rate is below the maximal conversion rate [1]. Thus, for wideband applications that cannot afford the size or expense of an optical system, the multicoset sampling becomes impractical. Another limitation of multicoset sampling, which also exists in the optical implementation, is maintaining accurate time delays between the ADCs of different cosets. Any uncertainty in these delays hobbles the recovery from the sampled sequences.

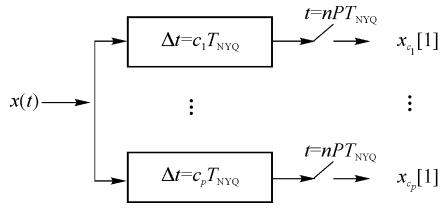

Fig. 1 Schematic implementation of multicoset sampling

2.2 AIC architecture design

2.2.1 CS theory

CS provides a framework for acquisition of a discrete-time signal which is sparse or compressible in somewhat sparsity basis. It is supposed that $x\in\mathbb{R}^N$ is an N-point real-valued discrete-time signal. Then $\boldsymbol{x}$ can be represented in an arbitrary basis $\{\psi_i\}_{i=1}^{N}$ for $\mathbb{R}^N$ with the weighting coefficients $\{\theta_i\}_{i=1}^{N}$. The signal $\boldsymbol{x}$ is represented as $\boldsymbol{x}=\sum_{i=1}^{N}\theta_i\psi_i=\boldsymbol{\Psi\Theta}$, where $\boldsymbol{\Psi}$ is an $N\times N$ matrix using ψ_i as columns, $\boldsymbol{\Theta}$ is the coefficient vector composed by the coefficients $\{\theta_i\}_{i=1}^{N}$. A signal is K-sparse in the basis $\boldsymbol{\Psi}$ if only K ($K\ll N$) significant elements are nonzero.

The useful information in the compressed signal can be captured by the non-adaptive linear projection. The random measurement for K-sparse signal $\boldsymbol{x}$ can be expressed as $\boldsymbol{y}=\boldsymbol{\Phi x}=\boldsymbol{\Phi\Psi\Theta}$, where $\boldsymbol{y}$ is an $M\times1$ vector and $\boldsymbol{\Phi}$ is an $M\times N$ ($M\ll N$) matrix. In order to recover the original signal $\boldsymbol{x}$, the matrix $\boldsymbol{A}=\boldsymbol{\Phi\Psi}$ must satisfy the restricted isometry properties (RIP) [2]. That is, the measurement matrix $\boldsymbol{\Phi}$ must be incoherent with the

sparse basis $\boldsymbol{\Psi}$. In practical applications, the elements of $\boldsymbol{\Phi}$ are independently drawn from a random distribution.

Recovering $\boldsymbol{x}$ from $\boldsymbol{y}$ is an ill-posed problem in general since M is far smaller than N. However, due to the additional assumption that the signal $\boldsymbol{x}$ is sparse or compressible in the basis $\boldsymbol{\Psi}$, measurements should be sufficient to make recovery both feasible and practical. The recovery of the sparse set of significant coefficients $\boldsymbol{\Theta}$ can be achieved through l_0-norm optimization. While solving this l_0-norm optimization is a NP-hard problem, we can get the solution of the problem through transforming the l_0-norm optimization into the l_1-norm optimization as:

$$\left.\begin{aligned} &\min \|\boldsymbol{\Theta}\|_1 \\ &\text{s.t.} \\ &\boldsymbol{y}=\boldsymbol{\Phi}\boldsymbol{\Psi}\boldsymbol{\Theta} \end{aligned}\right\} \tag{2}$$

This convex optimization problem, also known as basis pursuit (BP) [9], can be simplified to a traditional linear programming problem. An alternative to the optimization-based approach is greedy algorithm based on dynamic programming, such as matching pursuit (MP) [10] and orthogonal matching pursuit (OMP) [11– 12].

2.2.2 Random modulation preintegration (RMPI)

The RMPI structure is shown in Fig. 2. It multiplies the signal by a pseudo-random sequence of ± 1 s, integrates the product over the signal period T, and digitizes the integral at the end of each time interval. It implies that the sampling device has a number of parallel branches of mixers and integrators (BMIs) in order to process the analog signal in real-time.

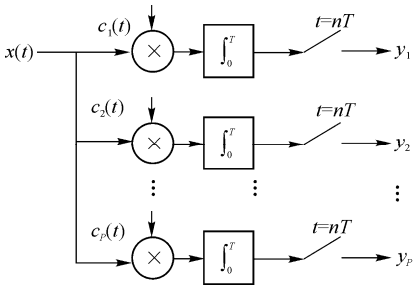

Fig. 2 The structure of the AIC based on RMPI

System performance depends largely on the number of samples. Thus, the larger the number of samples, the better recovery performance can be achieved in the noisy case. In order to collect a larger number of compressed samples using the AIC structure in Fig. 2, we need to increase the hardware complexity by adding more BMIs, which makes the AIC device more complex although its sampling rate is much lower than that of the traditional ADC based on the Nyquist theorem.

2.2.3 PSCS structure

In order to reduce the number of parallel BMIs in the AIC based on RMPI without sacrificing significantly the signal recovery accuracy, it can be achieved by adding to the AIC the capability of sampling at a higher rate, which is, however, still significantly lower than the sampling rate required by the ADC. The latter can be achieved by splitting the integration period T in every BMI of the AIC in Fig. 2 into many shorter sub-periods (segments). This system can be called as PSCS, which is shown in Fig. 3.

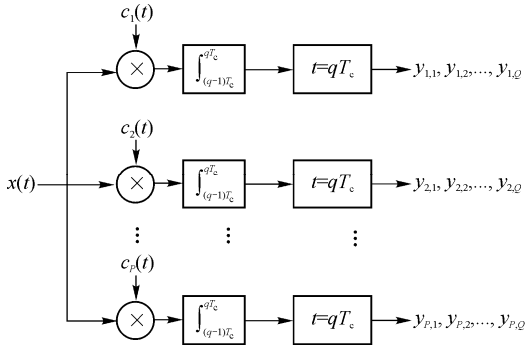

Fig. 3 The PSCS structure of AIC

The input signal is fed into parallel paths and each path is associated with a pseudo chipping sequence with value ±1 which chipping rate must be faster than the Nyquist rate. Then the demodulated signal is piecewise integrated and is sampled at a sub-Nyquist rate in each path.

Assuming the original signal period is T and the sampling rate in each path is $1/T_c$, then $Q=\text{int}(T/T_c)$ subsamples are obtained in each path, where function $\text{int}(\cdot)$ means a rounding down action. In PSCS system, the signal is integrated during every sampling time interval and the integrator must be reset after every piecewise integral. So the reset frequency of the integrator is high and equal to the sampling frequency.

Fig. 3 shows the idea of traditional PSCS where the input signals are segmented. However it is still difficult to be implemented physically because of the necessity of many multipliers and integrators. Furthermore the integrator and low speed ADC must be synchronous strictly, otherwise the performance of PSCS will be reduced.

3 Multi-rate sub-Nyquist sampling system

3.1 The structure of MSS system

The PSCS structure consumes much hardware resources, so that the high reset frequency of integrator will result in high power consumption. In order to reduce the hardware resource consumption and power consumption, the authors proposed a new sampling system called MSS system. The MSS architecture of AIC is described in Fig. 4. Compared to PSCS structure, it still consists of three main components, but becomes simpler and only needs one multiplier and one integrator.

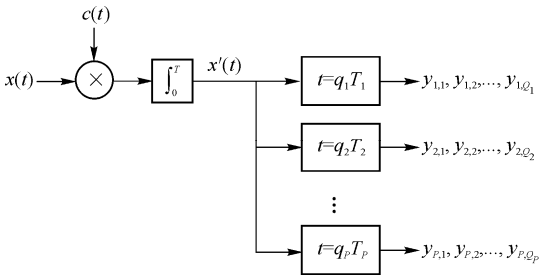

Fig. 4 The MSS architecture of AIC

The input signal $x(t)$ is firstly multiplied by a pseudo chipping sequence $c(t)$. Then the demodulated signal is integrated during every signal period T and the output of integrator $x'(t)$ is given as:

$$x'(t)=\int_0^t x(\tau)c(\tau)\mathrm{d}\tau;\quad 0\leqslant t\leqslant T \tag{3}$$

Finally the integrated signal is fed into parallel ADCs to sample at the different sub-Nyquist rates.

Amusing P ADCs are needed and the sampling interval of the pth ADC is T_p, then $Q_p=\mathrm{int}(T/T_p)$ subsamples are obtained during signal period T by the pth ADC. The output $y_{p,q}$ in the q_pth sampling interval of pth ADC is given as:

$$y_{p,q}=x'(t)|_{t=q_pT_p}=\int_0^{q_pT_p}c(\tau)x(\tau)\mathrm{d}\tau=\sum_{i=1}^{N}\theta_i\int_0^{q_pT_p}c(\tau)\psi_i(\tau)\mathrm{d}\tau \tag{4}$$

where $1\leqslant p\leqslant P$, $1\leqslant q_p\leqslant Q_p$. So there are $M=Q_1+Q_2+\cdots+Q_P$ subsamples obtained by the MSS system. In order to make every subsample has new information, any two sampling periods cannot be multiple relationships. That is $T_{i'}\neq kT_{j'}$ $(i'\neq j';1\leqslant i',j'\leqslant p;k=1,2,\cdots)$.

Table 1 shows the comparison between RMPI, PSCS and MSS, assuming P ADCs are adopted by these three structures.

Table 1 The features of RMPI, PSCS and MSS when P ADCs are adopted by these three structures

Structure	Demodulation	Integration	Sampling	Number of subsamples
RMPI	P sequences and P multipliers	P integrator and the integration period is T	P ADCs which have the same sampling intervals	P
PSCS structure	P sequences and P multipliers	P integrator and the integration period is T_c	P ADCs which have the same sampling intervals	About $P\left(\frac{T}{T_c}\right)$
MSS structure	One sequence and one multiplier	One integrator and the integration period is T	P ADCs which have the different sampling intervals	About $P\left(\frac{T}{T_1}+\cdots+\frac{T}{T_P}\right)$

3.2 Recovery from subsamples

It is known from Eq. (4) that the subsample contains the information obtained by the previous one and the new information which have not been captured. By appropriate processing of subsamples, repeating information contained in each subsample can be removed and only new informationis leaved. Then the whole measurement process is completed.

Steps of recovery from subsamples are elaborated as follows:

Step 1 Sort the subsamples in chronological order and get a new vector $\boldsymbol{Y}_s'$:

Define $\boldsymbol{T}_s=[T_1,...,Q_1T_1,T_2,...,Q_2T_2,...,T_P,...,Q_PT_P]^{\mathrm{T}}$, $\boldsymbol{Y}_s=[y_{1,1},...,y_{1,Q_1},y_{2,1},...,y_{2,Q_2},...,y_{P,1},...,y_{P,Q_P}]^{\mathrm{T}}$, then sort $\boldsymbol{T}_s$ in chronological order $[\boldsymbol{T}_s',\boldsymbol{P}_s]=\mathrm{sort}(\boldsymbol{T}_s)$, where function $\mathrm{sort}(\cdot)$ means the elements are ordered chronologically, $\boldsymbol{T}_s'$ is the ordered vector and $\boldsymbol{P}_s$ is the index vector. The chronologically ordered vector $\boldsymbol{Y}_s'$ is obtained as $\boldsymbol{Y}_s'=\boldsymbol{Y}_s(\boldsymbol{P}_s)$, which means the subsamples vector is sorted by the index vector $\boldsymbol{P}_s$.

It usually occurs that some elements of $\boldsymbol{T}_s$ may take same value, which means ADCs sampling at same instant. This leads to that the sampling is redundant and a sufficient number of effective samples may be not obtained. In order to let elements be with same value less, the lowest common sampling instant of any two ADCs should be large and any two ADCs' sampling rate should not satisfy the multiple relationship.

Step 2 Construct a new column vector $\hat{\boldsymbol{Y}}_s$, where the

mth element $\hat{\boldsymbol{Y}}_{\mathrm{s}}(m)$ is obtained by

$$\hat{Y}_{\mathrm{s}}(m)=\begin{cases}Y_{\mathrm{s}}'(m); & m=1\\ Y_{\mathrm{s}}'(m)-\boldsymbol{Y}_{\mathrm{s}}'(m-1); & 1<m\leqslant M\end{cases} \tag{5}$$

where $Y_{\mathrm{s}}'(m)$ is the mth element of $\boldsymbol{Y}_{\mathrm{s}}'$. For brief, it is can be defined as $\boldsymbol{Y}_{\mathrm{s}}'(0)=0$. Then Eq. (4) can be simplified as $\hat{Y}_{\mathrm{s}}(m)=Y_{\mathrm{s}}'(m)-Y_{\mathrm{s}}'(m-1),\quad 1\leqslant m\leqslant M$. According to Eqs. (4) and (5), $\hat{Y}_{\mathrm{s}}(m)$ can be further expressed as:

$$\begin{aligned}\hat{Y}_{\mathrm{s}}(m)=Y_{\mathrm{s}}'(m)-Y_{\mathrm{s}}'(m-1)=&\sum_{i=1}^{N}\theta_i\int_0^{T_{\mathrm{s}}'(m)}c(\tau)\psi_i(\tau)\mathrm{d}\tau-\\ &\sum_{i=1}^{N}\theta_i\int_0^{T_{\mathrm{s}}'(m-1)}c(\tau)\psi_i(\tau)\mathrm{d}\tau=\\ &\sum_{i=1}^{N}\theta_i\int_{T_{\mathrm{s}}'(m-1)}^{T_{\mathrm{s}}'(m)}c(\tau)\psi_i(\tau)\mathrm{d}\tau\end{aligned} \tag{6}$$

where $\boldsymbol{T}_{\mathrm{s}}'(m)$ is the mth element of $\boldsymbol{T}_{\mathrm{s}}'$.

Step 3 For brevity, we define the $M\times N$ matrix $\mathbf{V}=\boldsymbol{\Phi\Psi}$. According to Eq. (6), the element of $\boldsymbol{V}$ in the mth row and the ith column can be expressed as:

$$v_{m,i}=\int_{T_{\mathrm{s}}'(m-1)}^{T_{\mathrm{s}}'(m)}c(\tau)\psi_i(\tau)\mathrm{d}\tau \tag{7}$$

Step 4 The analog signal $x(t)$ can be finally recovered by solving the following problem

$$\left.\begin{aligned}&\min\|\boldsymbol{\Theta}\|_1\\ &\text{s.t.}\\ &\hat{\boldsymbol{Y}}_{\mathrm{s}}=\boldsymbol{V\Theta}\end{aligned}\right\} \tag{8}$$

In this article, the OMP algorithm was adopted to solve Eq. (8) and the sparse vector $\boldsymbol{\Theta}$ was got.

4 Performance analysis

In this section, simulations show effectiveness of the MSS structure where the input signals are time-frequency signals which are modulated using different frequencies at different time, as in the case of frequency hopping radios.

The short-time Fourier transforms (STFT) that performs Fourier analysis of windowed versions of the input signals to establish frequency content at local time neighborhoods is used to analyses this class of signals. The STFT is written as

$$\alpha(t,f)=\left\langle x,\psi_{t,f}\right\rangle=\int_{-\infty}^{+\infty}x(t)g(t-\tau)\,\mathrm{e}^{-\mathrm{j}2\pi ft}\mathrm{d}\tau \tag{9}$$

where $g(\cdot)$ is a window function with $\|g\|_2=1$. This formulation allows us to track changes in frequency over time. We will use a dictionary of Gabor atoms during the reconstruction of the signal to obtain a representation directly in the time frequency domain. Thus, by using such a dictionary during CS reconstruction we obtain a spectrogram as the resulting representation. The spectrogram of the time-frequency signal composed of two frequencies which are selected randomly on $[0, f_{\mathrm{NYQ}}/2]$ where $f_{\mathrm{NYQ}}=200$ MHz. In order to reflect the system performance of AIC, the detection percentage (DP) is exploited, where DP is expressed as:

$$P_{\mathrm{DP}}=\left(1-\frac{\|\tilde{\boldsymbol{\Theta}}-\boldsymbol{\Theta}\|}{\|\boldsymbol{\Theta}\|}\right)\times 100\% \tag{10}$$

Taking simulations on the performances under different conditions, all examples show that the performance will be better with high signal to noise ratio (SNR). When the multicoset sampling is adopted, the accurate time delay is about $1/f_{\mathrm{NYQ}}=5$ ns, which makes it difficult to implement on hardware.

The performance of MSS structure which has only one ADC is shown in Fig. 5. In this simulation, MSS is equivalent to RMPI which also has one BMI. It is shown that better performance will be obtained if higher sampling rate is adopted. The MSS structure has stable performance when the sampling rate higher than 90 MHz which is about of 45% of the Nyquist sampling rate.

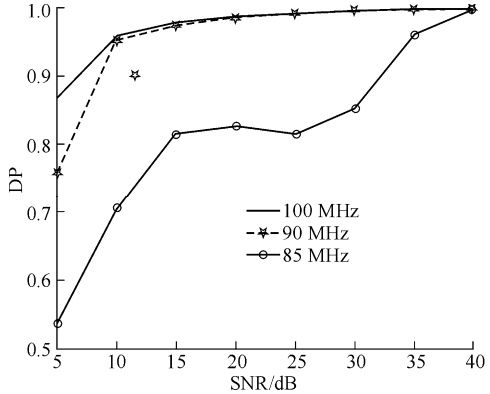

Fig. 5 The performances of MSS structure with only one ADC

Fig. 6 shows the performances of MSS structure with different ADCs. In example 1, the MSS structure has three ADCs which sampling rates are {30 MHz; 40 MHz; 50 MHz}. In example 2, the MSS structure has two ADCs whose sampling rates are {50 MHz; 70 MHz} and the MSS structure also has two ADCs whose ampling rates are {50 MHz; 60 MHz} in example 3. It is shown that the better performance will be obtained with higher sampling rate if the same number of ADCs is used. The highest

sampling rates in example 2 and example 3 are much lower, which are about 35% and 30% of the Nyquist sampling rate. Example 1 and example 2 have the similar performances, where they use different number of ADCs. In order to obtain similar performance, the sampling rates can be reduced if more ADCs are adopted. In example 1, the highest sampling rate is only about 25% of the Nyquist sampling rate, which is much lower than that in example 2.

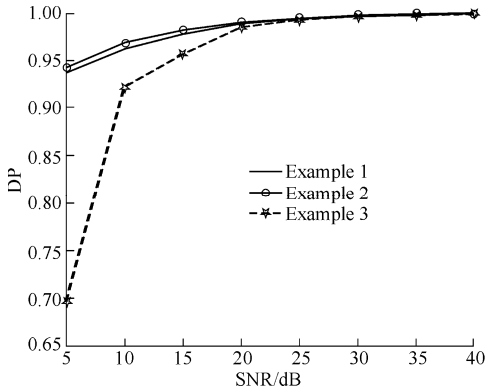

Fig. 6 The performances of MSS structure with different ADCs

Fig. 7 shows the comparison between RMPI, PSCS and MSS when they have similar performances. The signal period is about 1.28 μs, so the sampling rate in RMPI structure is about 781 kHz, which is very lower than the Nyquist sampling rate. However in order to have a good performance, it has as large as 100 BMIs, which leads to a lot of resource consumptions. PSCS structure reduces the number of BMIs instead of increasing the sampling rate. In Fig. 7, PSCS has only 3 BMIs and the sampling rate is 45 MHz, which is still lower than the Nyquist sampling rate. The needed resources are much fewer than those of RMPI. MSS further reduces the resource consumptions, which only has one mixer, one integrator and three ADCs with sampling rates separately at {30 MHz; 40 MHz; 50 MHz } in Fig. 7.

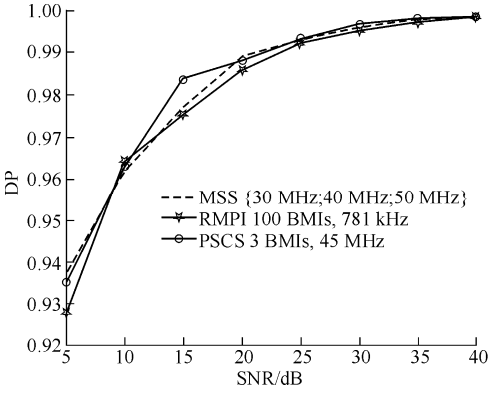

Fig. 7 Comparison between RMPI, PSCS and MSS when they have similar performances

Fig. 8 shows the performance of MSS under other conditions where three ADCs are used and two ADCs' sampling periods are multiple relationships. In example 1, the MSS structure has three ADCs and the sampling rates are {30 MHz; 40 MHz; 50 MHz} . So the total sampling rate is 120 MHz. In example 2, the three ADCs' sampling rates are {20 MHz; 30 MHz; 80 MHz} and the total sampling rate is 130 MHz. Though the total sampling rate in example 2 is higher than that of example 1 and more subsamples are obtained, the performance is worse than that of example 1. Because the sampling period of first ADC and that of third ADC are multiple relationships, so the subsamples obtained by the first ADC are fully redundant.

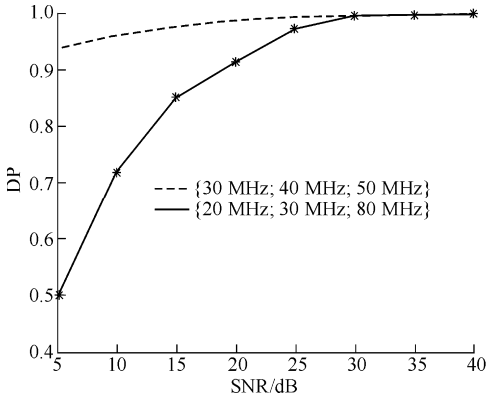

Fig. 8 The performances of MSS structure where two ADCs' sampling periods are multiple relationships

From these simulations, we can know that the MSS structure can reconstruct the original signals in high probability and needs fewer resources than RMPI and PSCS. However in order to obtain better performance, not only the total sampling rate are used, but also any two sampling periods cannot be multiple relationships to ensure less redundant subsamples.

5 Conclusions

A widen bandwidth is adopted in wireless communication to get high-speed data transmission. A MSS architecture of AIC was proposed to sample the analog signals at a sub-Nyquist rate. The original signals can be reconstructed in high probability when adopting the improved structure. Compared to the traditional RMPI and PSCS structure, this structure is simpler and consumes fewer resources. However in order to have better performance, the ADCs should be carefully chosen to make less redundant subsamples obtained.

Acknowledgements

This work was supported by the China Key Projects in the National Science and Technology (2012BAF14B01), the National Science and Technology Major Project of the Ministry of Science and Technology (2013ZX03001008), the National Natural Science Foundation of China (61322110), and the Program for New Century Excellent Talents in University of Ministry of Education of China (NCET-11-0598).

References

1. Venkataramani R, Bresler Y. Perfect reconstruction formulas and bounds on aliasing error in sub-Nyquist nonuniform sampling of multiband signals. IEEE Transactions on Information Theory, 2000, 46(6): 2173–2183
2. Candes E J, Wakin M B. An introduction to compressive sampling. IEEE Signal Processing Magazine, 2008, 25(2): 21–30
3. Donoho D. Compressed sensing. IEEE Transactions on Information Theory, 2006, 52(4): 1289–1306
4. Kirolos S, Ragheb T, Laska J, et al. Practical issues in implementing analog-to-information converters. Proceedings of the 6th International Workshop on System-on-Chip for Real-time Applications (WSOC'12), Dec 28–30, 2006, Cairo, Egypt. Piscataway, NJ, USA: IEEE, 2006: 141–146
5. Mishali M, Eldar Y C, Tropp J A. Efficient sampling of sparse wideband analog signals. Proceedings of the IEEE 25th Convention of Electrical and Electronics Engineers in Israel (IEEEI'08), Dec 3–5, 2008, Eilat, Israel. Piscataway, NJ, USA: IEEE, 2008: 290–294
6. Chen X, Yu Z, Hoyos S, et al. A sub-Nyquist rate sampling receiver exploiting compressive sensing. IEEE Transactions on Circuits and Systems I: Regular Papers, 2010, 58(3): 507–520
7. Mishali M, Eldar Y C. From theory to practice: sub-Nyquist sampling of sparse wideband analog signals. IEEE Journal of Selected Topics in Signal Processing, 2010, 4(2): 375–391
8. Zhao Y, Zhuang X, Wang H, et al. Model-based multichannel compressive sampling with ultra-low sampling rate. Circuits, Systems, and Signal Processing, 2012, 31(4): 1475–1486
9. Bazerque J A, Mateos G, Giannakis G B, et al. Basis pursuit for spectrum cartography. Proceedings of the 36th IEEE International Conference on Acoustics, Speech, and Signal Processing (ICASSP'11), May 22–27, 2011, Prague, Czech. Piscataway, NJ, USA: IEEE, 2011: 2992–2995
10. Nef R, Zakhor A. Sparse decomposition algorithm using immune matching pursuit. Proceedings of the 11th International Conference on Signal Processing (ICSP'12): Vol 1, Oct 21–25, 2012, Beijing, China. Piscataway, NJ, USA: IEEE, 2012: 489492
11. Joel A T, Anna C G. Signal recovery from random measurements via orthogonal matching pursuit. IEEE Transactions on Information Theory, 2007, 53(12): 4655–4666
12. Kaur A, Budhiraja S. Wavelet based sparse image recovery via orthogonal matching pursuit. Proceedings of the 2014 Recent Advances in Engineering and Computational Sciences (RAECS'14), Mar 6–8, 2014, Chandigarh, India. Piscataway, NJ, USA: IEEE, 2014: 5p

(Editor: Wang Xuying)

From p. 80

4. Zhang Y, Lian A Q, Luo Y. Wavelet transform and AR model based pattern recognition of EMG. Journal of Electronic Measurement and Instrument, 2011, 25(9): 770–774 (in Chinese)
5. Diab M O, Moslem B, Khalil M, et al. Classification of uterine EMG signals by using normalized wavelet packet energy. Proceedings of the 16th IEEE Mediterranean Electrotechnical Conference (MELECON'12), Mar 25–28, 2012, Yasmine Hammamet, Tunisia. Piscataway, NJ, USA: IEEE, 2012: 335–338
6. Qiu Q J, Zhu X Y. Feature extraction and pattern recognization of surface electromyography signal based on bispectrum analysis. Journal of Clinical Rehabilitative Tissue Engineering Research, 2010, 14(4): 645–648 (in Chinese)
7. Kamavuako E N, Farina D, Jensen W. Use of sample entropy extracted from intramuscular EMG signals for the estimation of force. Proceedings of the 15th Nordic-Baltic Conference on Biomedical Engineering and Medical Physics (NBC'11), Jun 14–17, 2011, Aalborg, Denmark. Berlin, Germany: Springer-Verlag, 2011: 125–128
8. Xi X G, Jin Y, Zhu H G, et al. EMG signal recognition based on EMD sample entropy. Journal of Central South University: Science and Technology, 2013, 44 (S2): 150–154 (in Chinese)
9. Zheng X, Chen W Z, Cui B Y. Multi-gradient surface electromyography (SEMG) movement feature recognition based on wavelet packet analysis and support vector machine (SVM). Proceedings of the 5th International Conference on Bioinformatics and Biomedical Engineering (iCBBE'11), May 10–12, 2011, Wuhan, China. Piscataway, NJ, USA: IEEE, 2011: 4p
10. Galiana-Merino J J, Ruiz-Fernandez D, Martinez-Espla J J. Power line interference filtering on surface electromyography based on the stationary wavelet packet transform. Computer Methods and Programs in Biomedicine, 2013, 111(2): 338–346
11. Yang X L, Li Z W, Hu Z G. The research of electromyographic signal based on sample entropy. China Science and Technology Information, 2014(2): 34–36 (in Chinese)
12. Hu Z F, Li L, Luo Y, et al. Human robot interaction based on head gesture. Journal of Chongqing University of Posts and Telecommunications: Natural Science, 2010, 22 (4): 492–495 (in Chinese)
13. Lee L K, An S Y, Oh S Y. Efficient face detection and tracking with extended CAMSHIFT and Haar-like features. Proceedings of the 2011 International Conference on Mechatronics and Automation (ICMA'11), Aug 7–10, 2011, Beijing, China. Piscataway, NJ, USA: IEEE, 2011: 507–513
14. Andrey O, Viacheslav N, Irina I, et al. Distributed system of real time head gesture recognition in development of contactless interfaces. Middle-East Journal of Scientific Research, 2014, 20 (12): 2177–2183
15. Gokce E I, Shrivastava A K, Cho J J, et al. Decision fusion from heterogeneous sensors in surveillance sensor systems. IEEE Transactions on Automation Science and Engineering, 2011, 8(1): 228–233

(Editor: Wang Xuying)